SHORT COMMUNICATIONS

DIFFUSION-WEIGHTED MAGNETIC RESONANCE IMAGING IN NON-INVASIVE MONITORING OF ANTIANGIOGENIC THERAPY IN EXPERIMENTAL TUMOR MODEL

S.A. Kharuzhyk[1,]*, N.A. Petrovskaya[2], M.A. Vosmitel[3]

[1]*Department of Diagnostic Radiology, [2]Department of Hyperthermia and Photodynamic Therapy, [3]Department of Pathology, N.N. Alexandrov National Cancer Center of Belarus, BY 223040 Lesnoj 2, Minsk, Belarus*

Aim: To show usefulness of diffusion-weighted magnetic resonance imaging (MRI) for non-invasive assessment of experimental tumor after antiangiogenic treatment. *Methods:* M1 sarcoma was implanted to the peritoneal cavity of the rat and allowed to grow to a palpable tumor size. Animal was treated with a single injection of endothelial growth factor antibody Bevacizumab (Avastin). Serial MRI scanning including diffusion-weighted sequence was performed before and up to 100 h after treatment. Animal was sacrificed thereafter and MRI data were correlated with morphology. *Results:* Apparent diffusion coefficient (ADC) maps derived tumor necrotic area correlated well with histology-derived tumor necrotic area. ADC threshold of 1.39×10^{-3} mm^2/s appeared to be optimal for tumor necrosis quantification in this tumor model and allowed to follow temporal changes of tumor internal structure after treatment. *Conclusion:* Diffusion-weighted MRI permits non-invasive tissue characterization without the need for exogenous contrast agents and, therefore, may be used to individualise therapy and to monitor tumor response.
Key Words: diffusion-weighted magnetic resonance imaging, peritoneal carcinomatosis, antiangiogenic therapy, non-invasive assessment.

Magnetic resonance imaging (MRI) is widely used in diagnostics of malignant tumors and evaluation of anticancer treatment efficacy bough in human and experimental models. T2- and T1-weighted images are routinely applied, providing information about size and internal structure of tumor, its relationship with surrounding tissues, the presence and severity of contrast enhancement. In addition to these anatomical MRI techniques, so called "functional" sequences has been developed in recent years. In functional MRI unique pathophysiological features of tissues are used for creation of images such as blood flow changes (ischemia, angiogenesis) in perfusion MRI and changes in the cellular composition (hypercellularity, necrosis) in diffusion-weighted MRI (DWI).

Initially DWI has been applied for early diagnostics of brain ischemia [1]. Cytotoxic edema develops immediately after blood flow shut down in the affected region of the brain. It characterized by fluid flow into intracellular space followed by cells swelling and decreasing of free mobility of water molecules in the constricted extracellular space. These areas with decreased water diffusion have altered signal on diffusion-weighted images, allowing to identify ischemia several hours earlier than on T2-weighted images. In recent years, it has been found that solid tumors are also characterized by decreased diffusion as they usually have increased cellular density. In opposite, areas of necrosis have increased diffusion due to absence of cell membranes as barriers for mobility of water molecules [2].

DWI has been used to detect tumors [3], to differentiate benign from malignant tumor types [4], and to detect diffusion changes after tumor therapy in human [5] and animal models [2, 6]. For assessment of antiangiogenic drugs therapies, DWI offers an attractive alternative to anatomic size measurements and/or histopathology because changes in size may not correlate with therapeutic efficacy, size changes may occur with significant delay relative to functional changes in tumor physiology and the invasive nature of histopathology complicates longitudinal studies. An important advantage of DWI is the possibility of quantitative assessment by constructing map of the apparent diffusion coefficient (ADC map). In the present work we demonstrate use of DWI for non-invasive assessment of tumor internal structure changes in experimental model of peritoneal carcinomatosis treated with antiangiogenic drug Avastin with morphologic correlation.

Tumor model. Animal experiments were conducted in compliance with all ethical and legal requirements. An experimental animal, a white rat, was obtained from the vivarium of the N.N. Alexandrov National Cancer Center of Belarus. M-1 sarcoma, a transplantable rat tumor, was used in the experiments. The strain was obtained from the Oncology Research Centre of the Russian Academy of Medical Sciences and was passed by serial transplantation. Tumor nodes were isolated and homogenized, then Hank's solution was added to yield 10% suspension. The tumor cell suspension was injected under the capsule of the peritoneal surface in the left lower side of the abdomen.

MRI scanning and treatment. Baseline MRI scan was performed under general anesthesia 19 days after tumor transplantation and consisted of coronal and transversal T2- and T1-weighted images followed by DWI in transversal plane. Positions and thickness (3 mm) of DWI slices were copied from transversal T2-weighted images which served as anatomic reference. Four central tumor slices were underwent future quantitative analysis in correlation with histology.

Immediately after MRI Bevacizumab (Avastin) endothelial growth factor antibody (Genentech Inc., South San Francisco, CA) was injected in tail vein in dose 15 mg/kg. Animal was undergone to MRI for noninvasive monitoring at 24, 48, 80 and 100 h after single dose Avastin injection using the same scanning protocol as described above.

Morphology examination. To validate the data of MRI animal was sacrificed after last MRI examination (according to the regulations of local Ethic Committee). At necropsy, the tumor was removed and fixed in 10% neutral buffered formalin for over 24 h. Four transversal parallel 3 mm thick sections were obtained through center of the tumor in correspondence to transversal DWI and T2-weighted images of MRI. H&E staining was done using standard protocols of histology investigation. Regions of necrosis were demarcated on the digital photo of the histology sections and percentage of necrotic tumor area was calculated for each section.

ADC maps analysis. ADC maps were reconstructed from DWI series using scanner software. Diffusion-weighted images and ADC maps have lower spatial resolution and, thus, are interpreted together with T2- and T1-weighted images, which serve as anatomic reference. On the ADC map signal intensity of each pixel corresponds to the diffusion coefficient at this point. Necrotic areas which are characterized by increased diffusion have increased signal (appears white) while solid tumor parts look dark. To analyze ADC maps quantitatively ImageJ program (NIH, Bethesda, USA) was used. Tumor node was contoured and ADC threshold was found for which the total area of pixels in each slice with the intensity of the signal above the threshold value (ADC-derived tumor necrotic area) best suited to the area of necrosis in corresponding morphology slice (histology-derived tumor necrotic area). Sum of square differences (SSD) technique was used to find an optimal threshold [7]. The optimal threshold value was determined as that which yield the minimum SSD between ADC- and histology-derived tumor necrotic areas on four analyzed tumor slices. As shown in Fig. 1 minimum SSD was obtained with ADC threshold of 1.39×10^{-3} mm^2/s. Fig. 2 shows correlation plots of ADC- and histology-derived tumor necrotic areas estimated using representative ADC thresholds of 1.35, 1.39 and 1.41×10^{-3} mm^2/s relative to the model x = y line. Threshold of 1.35×10^{-3} mm^2/s overestimates tumor necrosis compared to histology while threshold of 1.41×10^{-3} mm^2/s underestimates it. Using optimal ADC threshold of 1.39×10^{-3} mm^2/s, percentage of ADC-derived tumor necrotic area on each of four slices was 21.1, 16.4, 15.7 and 28.8%, showing excellent correspondence to 21.1, 18.6, 15.9 and 28.6% on histology respectively. MRI and pathology images from representative tumor slice are shown on Fig. 3.

ADC maps analysis allowed to follow temporal changes of tumor internal structure after treatment. ADC-derived tumor necrotic volume increased gradually from 6.7% before treatment to 11.6% at 48 h and up to 27.7% at 80 h after Avastin injection.
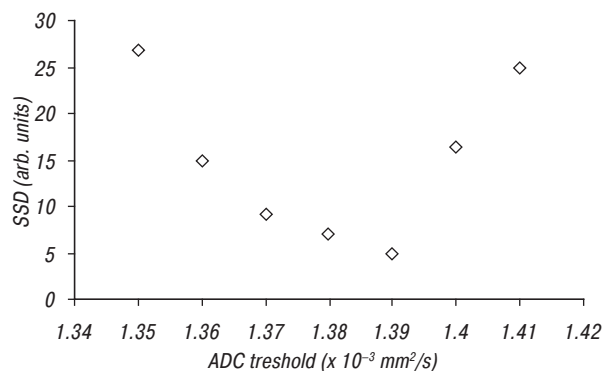

Fig. 1. Plot of sum of square differences (SSD) of ADC- and histology-derived tumor necrotic areas on four slices versus ADC threshold. Minimal SSD value was achieved with ADC threshold of 1.39×10^{-3} mm^2/s indicating best correspondence of ADC- and histology derived tumor necrotic areas
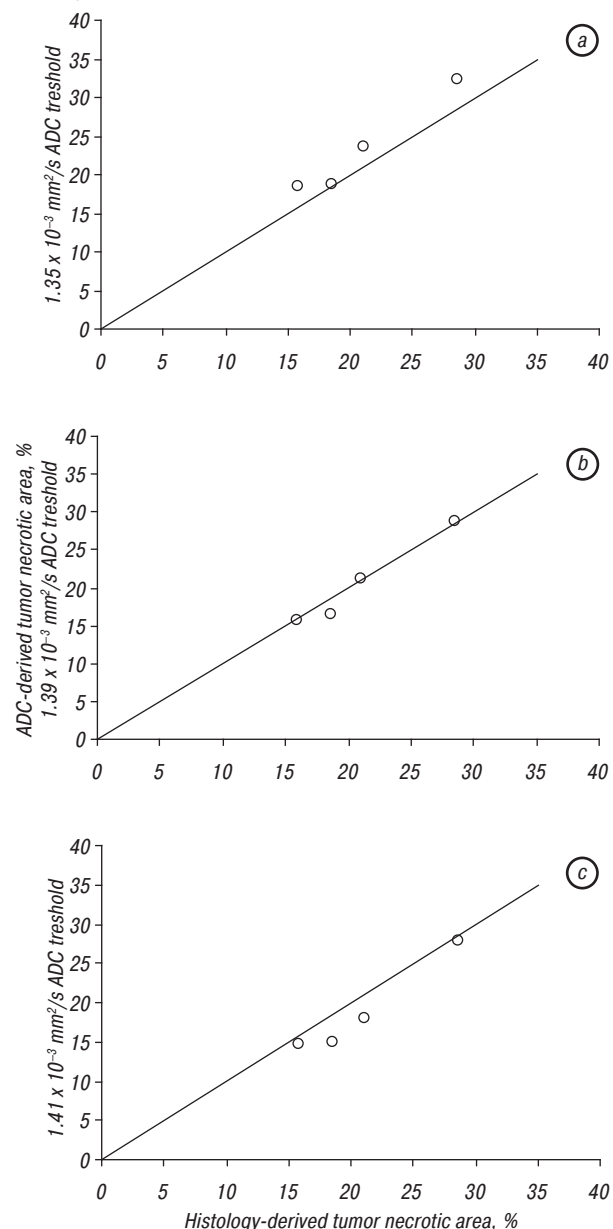

Fig. 2. Correlation plots between ADC- and histology-derived tumor necrotic areas relative to the model x = y line. Every point on the plot corresponds to individual tumor slice. Representative ADC thresholds of (*a*) 1.35, (*b*) 1.39 and (*c*) 1.41×10^{-3} mm^2/s are shown. The best correspondence of ADC-derived and histology-derived tumor necrotic areas is achieved with ADC threshold of 1.39×10^{-3} mm^2/s
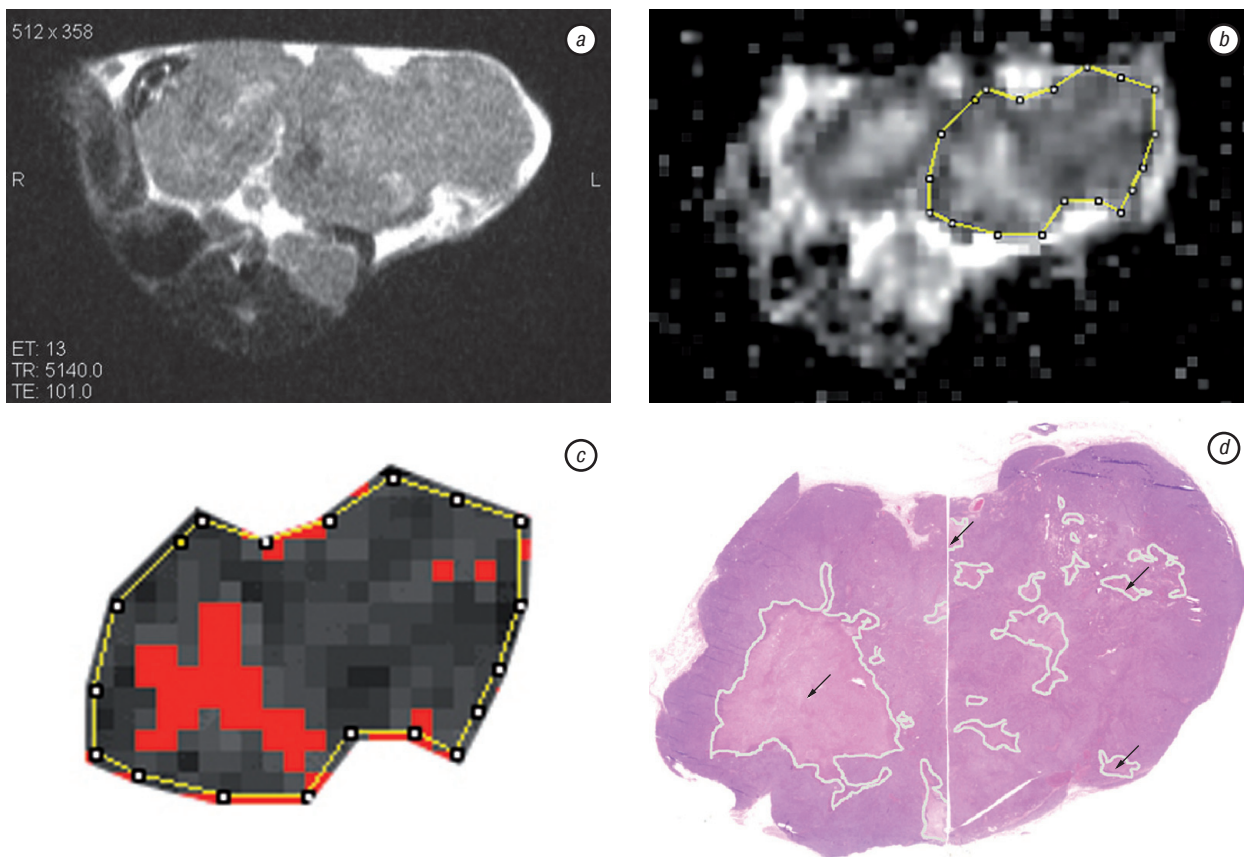
Fig. 3. MRI (*a*–*c*) and histology (*d*) images from representative slice of M1-sarcoma at 100 h post treatment with Avastin: (*a*) T2-weighted image and (*b*) ADC map of the experimental animal whole body transversal cross-section; (*c*) ADC map and (*d*) H&E stained section of evaluated tumor node which is delineated on (*b*). Red pixels on (*c*) represent ADC values above 1.39×10^{-3} mm^2/s threshold which appeared optimal for discrimination of solid and necrotic areas on this tumor model. White areas in the tumor on (*b*) and red pixels on (*c*) excellently match necrotic areas in the H&E stained section (arrows on (*d*)) as opposed to T2-weigted image on which tumor necrosis is not easily appreciated

In conclusion, DWI uses local water mobility as an endogenous probe for noninvasive interrogation of tissue microstructure and may permit tissue characterization without the need for exogenous contrast agents. It offers non-invasive evaluation of tumor necrotic fraction before, during and after treatment and, therefore, may be used to individualise therapy and to monitor tumor response.

REFERENCES

1. **Moseley ME, Kucharczyk J, Mintorovitch J, *et al*.** Diffusion-weighted MR imaging of acute stroke: correlation with T2-weighted and magnetic susceptibility-enhanced MR imaging in cats. Am J Neuroradiol 1990; **11**: 423–9.

2. **Deng J, Virmani S, Young J, *et al*.** Diffusion-weighted PROPELLER MRI for quantitative assessment of liver tumor necrotic fraction and viable tumor volume in VX2 rabbits. J Magn Reson Imaging 2008; **27**: 1069–76.

3. **Naganawa S, Sato C, Kumada Y, *et al*.** Apparent diffusion coefficient in cervical cancer of the uterus: comparison with the normal uterine cervix. Eur Radiol 2005; **15**: 71–8.

4. **Fujii S, Matsusue E, Kigawa J, *et al*.** Diagnostic accuracy of the apparent diffusion coefficient in differentiating benign from malignant uterine endometrial cavity lesions: initial results. Eur Radiol 2008; **18**: 384–9.

5. **Harry VN, Semple SI, Gilbert FJ, *et al*.** Diffusion-weighted magnetic resonance imaging in the early detection of response to chemoradiation in cervical cancer. Gynecol Oncol 2008; **111**: 213–20.

6. **Huang MQ, Pickup S, Nelson DS, *et al*.** Monitoring response to chemotherapy of non-Hodgkin's lymphoma xenografts by T2-weighted and diffusion-weighted MRI. NMR Biomed 2008; **21**: 1021–9.

7. **Kazemia M, Silva MD, Lib F, *et al*.** Investigation of techniques to quantify in vivo lesion volume based on comparison of water apparent diffusion coefficient (ADC) maps with histology in focal cerebral ischemia of rats. Magn Res Imaging 2004; **22**: 653–9.